

Test-retest reproducibility of quantitative binding measures of [¹¹C]Ro15-4513, a PET ligand for GABA_A receptors containing alpha5 subunits

Colm J. McGinnity^{a,b,c,*}, Daniela A. Riaño Barros^{a,b,1}, Lula Rosso^{a,b}, Mattia Veronese^d, Gaia Rizzo^e, Alessandra Bertoldo^e, Rainer Hinz^f, Federico E. Turkheimer^d, Matthias J. Koepp^{g,h}, Alexander Hammers^{a,b,c,i}

^a Centre for Neuroscience, Department of Medicine, Imperial College London, London, UK

^b Medical Research Council Clinical Sciences Centre, Hammersmith Hospital, London, UK

^c Division of Imaging Sciences & Biomedical Engineering, King's College London, London, UK

^d Centre for Neuroimaging Sciences, Institute of Psychiatry, Psychology & Neuroscience, King's College London, London, UK

^e Department of Information Engineering, University of Padova, Padova, Italy

^f Wolfson Molecular Imaging Centre, University of Manchester, Manchester, UK

^g Department of Clinical and Experimental Epilepsy, Institute of Neurology, University College London, UK

^h Epilepsy Society, Chalfont St Peter, UK

ⁱ The Neurodis Foundation, CERMEP - Imagerie du Vivant, Lyon, France

ARTICLE INFO

Keywords:

GABA_A
α5
Alpha5
Positron emission tomography
Reliability
Reproducibility

ABSTRACT

Introduction: Alteration of γ-aminobutyric acid “A” (GABA_A) receptor-mediated neurotransmission has been associated with various neurological and psychiatric disorders. [¹¹C]Ro15-4513 is a PET ligand with high affinity for α5-subunit-containing GABA_A receptors, which are highly expressed in limbic regions of the human brain (Sur et al., 1998). We quantified the test-retest reproducibility of measures of [¹¹C]Ro15-4513 binding derived from six different quantification methods (12 variants).

Methods: Five healthy males (median age 40 years, range 38–49 years) had a 90-min PET scan on two occasions (median interval 12 days, range 11–30 days), after injection of a median dose of 441 MegaBequerels of [¹¹C]Ro15-4513. Metabolite-corrected arterial plasma input functions (parent plasma input functions, ppIFs) were generated for all scans.

We quantified regional binding using six methods (12 variants), some of which were region-based (applied to the average time-activity curve within a region) and others were voxel-based: 1) Models requiring arterial ppIFs – regional reversible compartmental models with one and two tissue compartments (2kbv and 4kbv); 2) Regional and voxelwise Logan's graphical analyses (Logan et al., 1990), which required arterial ppIFs; 3) Model-free regional and voxelwise (exponential) spectral analyses (SA; (Cunningham and Jones, 1993)), which also required arterial ppIFs; 4) methods not requiring arterial ppIFs – voxelwise standardised uptake values (Kenney et al., 1941), and regional and voxelwise simplified reference tissue models (SRTM/SRTM2) using brainstem or alternatively cerebellum as pseudo-reference regions (Lammertsma and Hume, 1996; Gunn et al., 1997).

To compare the variants, we sampled the mean values of the outcome parameters within six bilateral, non-reference grey matter regions-of-interest. Reliability was quantified in terms of median absolute percentage test-retest differences (MA-TDs; preferentially low) and between-subject coefficient of variation (BS-CV, preferentially high), both compounded by the intraclass correlation coefficient (ICC). These measures were compared between variants, with particular interest in the hippocampus.

Results: Two of the six methods (5/12 variants) yielded reproducible data (i.e. MA-TD < 10%): regional SRTMs and voxelwise SRTM2s, both using either the brainstem or the cerebellum; and voxelwise SA. However, the

Abbreviations: BP_{ND}, binding potential relative to non-displaceable binding; BS-CV, between-subject coefficient of variation; FBP, filtered backprojection; FORE, Fourier rebinning; GABA_A, γ-aminobutyric acid “A” receptor; ICC, intraclass correlation coefficient; MAPER, multi-atlas propagation with enhanced registration; NHS, National Health Service (of the United Kingdom); MA-TD, median absolute percentage test – retest difference; NNLS, non-negative least squares; ppIFs, metabolite-corrected, arterial parent plasma input functions; ROI, region-of-interest; RPM, Receptor Parametric Mapping; SA, (exponential) spectral analysis; SRTM, simplified reference tissue model; SUV, standardised uptake values; TACs, time-activity curves; V_T, (total) volume-of-distribution; WS-CV, within-subject coefficient of variation

* Correspondence to: Division of Imaging Sciences & Biomedical Engineering, King's College London, 4th Floor Lambeth Wing, St. Thomas' Hospital, Westminster Bridge Road, London SE1 7EH, UK.

E-mail address: colm.mcginny@kcl.ac.uk (C.J. McGinnity).

¹ These authors contributed equally to this work.

<http://dx.doi.org/10.1016/j.neuroimage.2016.12.038>

Received 17 July 2016; Accepted 14 December 2016

Available online 11 March 2017

1053-8119/© 2016 The Author(s). Published by Elsevier Inc. This is an open access article under the CC BY license (<http://creativecommons.org/licenses/by/4.0/>).

SRTMs using the brainstem yielded a lower median BS-CV (7% for regional, 7% voxelwise) than the other variants (8–11%), resulting in lower ICCs. The median ICCs across six regions were 0.89 (interquartile range 0.75–0.90) for voxelwise SA, 0.71 (0.64–0.84) for regional SRTM-cerebellum and 0.83 (0.70–0.86) for voxelwise SRTM-cerebellum. The ICCs for the hippocampus were 0.89 for voxelwise SA, 0.95 for regional SRTM-cerebellum and 0.93 for voxelwise SRTM-cerebellum.

Conclusion: Quantification of [^{11}C]Ro15-4513 binding shows very good to excellent reproducibility with SRTM and with voxelwise SA which, however, requires an arterial ppIF. Quantification in the $\alpha 5$ subunit-rich hippocampus is particularly reliable. The very low expression of the $\alpha 5$ in the cerebellum (Fritschy and Mohler, 1995; Veronese et al., 2016) and the substantial $\alpha 1$ subunit density in this region may hamper the application of reference tissue methods.

1. Introduction

γ -aminobutyric acid (GABA) is one of the principal inhibitory neurotransmitters in the brain (Curtis et al., 1970). The ligand-gated, ion channel GABA_A receptor (Lobo and Harris, 2008) is a pentameric structure assembled from five of 19 known protein subunits: α_{1-6} , β_{1-3} , γ_{1-3} , δ , ϵ , π , ρ_{1-3} and θ (Barnard et al., 1998). On binding GABA, the permeability of the central pore to chloride ions increases, resulting in hyperpolarisation of the neuron and hence reduced excitability. The receptor subunits exhibit distinct but overlapping distributions within the brain (Fritschy and Mohler, 1995; Sieghart and Sperk, 2002) and roles that change during development and with pathologies (Galanopoulou, 2008).

Approximately 5% of GABA_A receptors contain the $\alpha 5$ subunit. The hippocampus is the structure with the highest concentration of $\alpha 5$ -subunit-containing receptors in the human brain; for example, an ex vivo study with the $\alpha 5$ -subunit-selective radioligand [^3H]L-655,708 suggested they are present in almost 28% of GABA_A receptors in this region (Sur et al., 1998). Here, they have a predominantly extrasynaptic localisation (Brunig et al., 2002) and mediate tonic inhibitory currents (Caraiscos et al., 2004). Experiments in animals suggest that agonists at receptors containing the $\alpha 5$ subunit negatively influence hippocampus-dependent learning and memory (Collinson et al., 2002; Crestani et al., 2002; Sternfeld et al., 2004; Yee et al., 2004; Cheng et al., 2006; Dawson et al., 2006). Whilst data in humans is lacking, the amnesic effect of alcohol on wordlist learning was reduced by pre-treatment with an $\alpha 5$ -subunit-selective inverse agonist (Nutt et al., 2007).

Alteration of GABA_A receptor-mediated neurotransmission has been associated with a wide variety of neurological and psychiatric disorders (Korpi and Sinkkonen, 2006), including alcohol dependence, anxiety (reviewed by Roy-Byrne (2005)), epilepsy ((Macdonald et al., 2004), reviewed by Gonzalez and Brooks-Kayal (2011)), and schizophrenia (reviewed by Charych et al. (2009)).

The synthesis of subtype-selective tracers such as Ro15-4513 (ethyl-8-azido-5,6-dihydro-5-methyl-6-oxo-4H-imidazo-1,4-benzodiazepine-3-carboxylate; F. Hoffmann–La Roche Ltd., Basel, Switzerland) promises further understanding of GABA_A receptors. Ro15-4513 is an $\alpha 5$ -subunit-selective imidazodiazepine that behaves as a partial inverse agonist at GABA_A receptors (Bonetti et al., 1988; Lister and Nutt, 1988; Sadzot et al., 1989). Receptors that express $\alpha 5$ subunits have 10–15-fold higher affinity to Ro15-4513 than those that do not (Hadingham et al., 1993; Luddens et al., 1994). Competition studies in the rat in vivo revealed that radiolabelled Ro15-4513 binding was reduced to nonspecific levels only by drugs that have affinity for the $\alpha 5$ subtype (flunitrazepam, RY80, Ro15-4513, L655,708) and that [^{11}C]Ro15-4513 has a tenfold higher affinity to $\alpha 5$ than $\alpha 1$ receptors (Lingford-Hughes et al., 2002).

In healthy human volunteers, pre-scan administration of the $\alpha 1$ antagonist zolpidem did not significantly decrease total [^{11}C]Ro15-4513 volume-of-distribution (V_T ; (Myers et al., 2012)), but alteration of the fast ($\alpha 1$) component peaks (derived using exponential spectral analysis; SA) was observed. In the $\alpha 5$ -rich hippocampus, the mean

volume-of-distribution attributable to the fast peaks was reduced by approximately 70% to 0.44, whereas a slower component (presumably attributable to the $\alpha 5$ subunit) was reduced by approximately 13% to 10.00. More recently, human heterologous competition data acquired from nine healthy males using the $\alpha 5$ -subunit-selective negative allosteric modulator, Basmisanil (RG1662), suggested that $\alpha 5$ -specific binding accounts for 76% of the specific binding in the hippocampus (Myers et al., 2016).

Inoue et al. (1992) used the simplified reference tissue model (SRTM) with pons as a (pseudo-) reference region to demonstrate the differences between the distribution of [^{11}C]Ro15-4513 and [^{11}C]flumazenil in five healthy participants. [^{11}C]Ro15-4513 V_T has also been previously quantified by voxel-wise exponential SA in three healthy males (Lingford-Hughes et al., 2002). Comparison with [^{11}C]flumazenil PET derived from six healthy males indicated significantly greater V_T (by approximately 36%) in the hippocampus for [^{11}C]Ro15-4513, with significantly less binding (approximately 43%) in the cerebellum.

[^{11}C]Ro15-4513 binding has also been quantified in eight healthy men using both compartmental modelling and linear graphical analyses (Asai et al., 2009); the SRTM with pons as a reference was recommended based on resilience to noise, but test – retest studies were not performed.

[^{11}C]Ro15-4513 PET has recently been used to demonstrate alterations in GABA_A $\alpha 5$ subunit binding in alcohol dependence (Lingford-Hughes et al., 2012), schizophrenia (Asai et al., 2008), in response to levodopa challenge (Lou et al., 2016), and in preliminary studies in temporal lobe epilepsy (Barros et al., 2010a) and autism spectrum disorder (Mendez et al., 2013). To facilitate interpretation, it is necessary to document the reproducibility and reliability of quantitative methods, both regional and voxelwise, for [^{11}C]Ro15-4513 PET. Whilst the test – retest variability of presumed $\alpha 1$ - and $\alpha 5$ -subunit-specific V_T has been reported (Stokes et al., 2014), the variability of total V_T has not. Moreover, the analysis performed by Stokes and colleagues was restricted to a single quantification method (SA), whereas variants that do not require an arterial input function, and variants which yield parametric images, still merit investigation. However, no such analysis has been published.

In the present study we quantified the test-retest reproducibility and reliability of measures of [^{11}C]Ro15-4513 binding derived from six quantification methods, namely standardised uptake values (SUVs), one tissue compartment and two tissue compartment models (2kbv and 4kbv), graphical (linear) analyses, SA, and SRTMs, in regions representative of a variety of $\alpha 5$ subunit concentrations, in five healthy volunteers.

2. Materials and methods

2.1. Participants

The study was approved by the London – Riverside National Health Service (NHS) Research Ethics Committee, Imperial College Healthcare NHS Trust, and University College London Hospitals

NHS Foundation Trust. Permission to administer [¹¹C]Ro15-4513 was obtained from the Administration of Radioactive Substances Advisory Committee, UK. All participants provided written, informed consent according to the Declaration of Helsinki prior to participation in the study.

Seven healthy male participants were recruited and provided written, informed consent. The exclusion criteria were: a history of either neurological or psychiatric condition(s), claustrophobia, any contraindication for undergoing magnetic resonance (MR) imaging, a positive urine drug test, general practitioner's (family doctor's) advice against participation, regular medication(s) (especially benzodiazepines), a history of substance abuse (especially benzodiazepines), and a pathological modified Allen's test for patency of the ulnar artery (Allen, 1929; Slogoff et al., 1983; Cable et al., 1999). Two of the seven participants were subsequently excluded: one who withdrew from the study before the second scan, and another in whom the arterial line could not be kept patent for the entire study. Hence, a total of five healthy male participants (median age 40 years, range 38–49 years; Table 1) were scanned twice. All participants underwent a urine drug cassette test for 11-nor- Δ^9 -tetrahydrocannabinol, morphine, amphetamine, benzoylecgonine (the main metabolite of cocaine), methamphetamine and oxazepam (Monitect; BMC, California, USA) on the same day as each PET scan.

2.2. Radiochemistry

[¹¹C]Ro15-4513 was produced on site by Hammersmith Imanet as described previously (Myers et al., 2012). Details of the injectate are provided in Table 1. Specific radioactivities at the time of injection were calculated in relation to the relative molecular weight of Ro15-4513 (326 mol/g).

2.3. PET data acquisition

PET scans were acquired on a Siemens/CTI ECAT EXACT HR +("962") camera (Knoxville, TN, USA; (Spinks et al., 2000)) in 3D mode. Ten-minute transmission scans for attenuation and scatter correction were obtained prior to the dynamic emission scans using a rotating ⁶⁸Ge rod source. Each dynamic acquisition was 90.5 min long and consisted of 24 frames of increasing length (1×30 s (s), 4×15 s, 4×60 s, 2×150 s, 10×300 s, 3×600 s). [¹¹C]Ro15-4513 was injected as an intravenous bolus injection of ~440 MegaBequerels (MBq; median 441 MBq, range 430–452 MBq; Table 1) at 30 s after the dynamic scan start. Participants were scanned on two separate days with a median interval of 12 days (range 7 – 59 days; Table 1).

Table 1
Demographic and injectate details for the participants.

Participant no.	Age	Gender	BMI	Interval (days)	Dose (MBq)	Radiochemical purity (%)	Co-injected mass (µg)	Specific Radioactivity (MBq/nmol)
1	40	M	25	12	431	99	2.0	72
					435	98	2.4	59
2	38	M	27	30	430	99	4.4	32
					437	98	2.2	66
3	39	M	20	11	447	99	3.0	49
					441	99	5.1	28
4	49	M	34	59	440	97	2.6	55
					442	98	3.5	42
5	44	M	23	7	452	96	3.0	26
					444	98	0.4	72
Median	40		25	12	441	98	2.8	52
Interquartile range (25th–75th perc)	39–44		23–27	11–30	435–443	98–99	2.2–3.4	34–64
Min	38		20	7	430	96	0.4	26
Max	49		34	59	452	99	5.1	72

BMI=Body mass index; MBq=MegaBequerels; Min=Minimum; Max=Maximum; µg=Micrograms; nmol=Nanomoles; no=Number; perc=Percentiles.

The head position was maintained throughout and monitored with the camera's positioning laser. To compensate for minor head movements during the dynamic scans, we used a post hoc frame-by-frame realignment method, as described later ("PET data quantification" section). Sixty-three transaxial images were acquired per frame. Data were reconstructed using Fourier rebinning (FORE; (Defrise et al., 1997)) and 2D filtered backprojection (FBP: ramp filter, kernel 2.0 millimetres (mm) Full Width at Half Maximum (FWHM)). The voxel size of reconstructed images was 2.092 mm×2.092 mm×2.42 mm and the axial (on-axis) resolution 5.6 mm (Spinks et al., 2000).

2.4. Input function derivation

As in previous studies, continuous and intermittent blood samples were collected to allow the subsequent generation of arterial parent plasma input functions (ppIFs; (Hammers et al., 2008; Riaño Barros et al., 2014)). During the first 15 min, blood was withdrawn continuously at a rate of 300 millilitres (ml) per hour and radioactivity detected in a bismuth germanium oxide detection system (Ranica et al., 1991). Intermittent discrete (10 ml) samples were taken using heparinised syringes before the scan (baseline) and at the following time points after the scan start: 4, 6, 8, 10, 20, 35, 50, 65, 80 and 90 min. These discrete samples were used to quantify plasma and whole blood radioactivity via centrifugation, as well as to allow quantification of the parent fraction of the radiotracer via high-performance liquid chromatography. The plasma-over-blood ratio model and the metabolite model were fit for each scan, so that the whole blood measurements between 0 and 15 min could be corrected for plasma-over-blood ratio and parent fraction, respectively. The plasma-over-blood ratio model used was as follows:

$$1 - \frac{x_1 + x_2 \cdot t_s}{(x_3/t_s)^{x_4} + 1} \quad (1)$$

[where t_s is the time from scan start in hours and x_1 to x_4 are the model parameters]. The same sigmoidal model function was used to describe the fraction of parent [¹¹C]Ro15-4513 remaining in plasma, as in (Myers et al., 2016).

Continuous ppIFs were derived using Clickfit in-house software running in MATLAB R2014a (The MathWorks, Natick, MA, USA), as described in detail in previous studies (Hammers et al., 2007b; Hinz et al., 2007):

- 1) Cross-calibration of continuous and discrete whole blood radioactivity concentration measurements (4, 6, 8, 10 min).
- 2) Multiplication of the cross-calibrated whole blood measurements (0–15 min) by the sigmoid function obtained from fitting the model

- to the plasma-over blood ratio.
- 3) Combination of the resultant continuous plasma radioactivity concentration curve (0–15 min) with the discrete plasma radioactivity concentration measurements (20, 35, 50, 65, 80 and 90 min) using spline interpolation.
 - 4) Correction for parent radiotracer fraction by multiplication of the resultant continuous plasma radioactivity concentration curve (0–90 min) by the sigmoid function obtained from fitting the model to the parent fraction.

2.5. MRI data acquisition, analysis and generation of regions-of-interest (ROIs)

All participants had 3D T1-weighted MRI scans with approximately millimetric isotropic voxel sizes on a Philips Intera 3 Tesla (3 T) MRI scanner (Philips, Best, The Netherlands) at the Robert Steiner MRI Unit, Hammersmith Hospital, for use during co-registration and region-of-interest (ROI) delineation. There was no gross structural abnormality on any of the T1-weighted images.

To isolate the grey matter in each brain, the T1-weighted images were segmented into tissue classes using SPM8 software (Statistical Parametric Mapping, Wellcome Trust Centre for Neuroimaging, University College London, London, www.fil.ion.ucl.ac.uk/spm) running in MATLAB R2014a. This process yielded grey matter probability maps for each participant, which were thresholded at 0.5 probability (an arbitrary value which was selected as a trade-off between over-exclusion of grey matter and over-inclusion of white matter).

To delineate the ROIs in each brain, the T1-weighted images were also anatomically segmented using MAPER (multi-atlas propagation with enhanced registration (Heckemann et al., 2010)). Using high-dimensional image registration, 30 MRI data sets, each associated with manually determined labels of 83 regions (Hammers et al., 2003; Gousias et al., 2008), were propagated to the target brain. Label fusion was used to obtain an image which consisted of 83 labelled ROIs in target space (Heckemann et al., 2006).

Each participant's T1-weighted image and corresponding MAPER-derived individual anatomical segmentations, as well as individual grey matter probability images, were co-registered with the corresponding processed PET summation image for test and retest scans separately, using SPM8. For the cortical ROIs, the individual atlases in PET space were then multiplied with the thresholded grey matter probability maps using Analyze 8.1 imaging software (Mayo Clinic 2002). The output grey-matter-masked, labelled ROI images were then used to sample the dynamic or parametric PET images.

2.6. ROIs

We evaluated test – retest reliability of the quantification methods (12 variants) in six bilateral ROIs in total. Based on the expected concentrations of GABA_A receptors containing $\alpha 5$ subunits, we selected ROIs to cover a range of binding: high-concentration limbic regions – anterior cingulate gyrus and hippocampus; intermediate concentration regions – fusiform (occipitotemporal) gyrus, inferior frontal gyrus and insula; and a low concentration region – the occipital lobes. The (entire) brainstem and alternatively the grey matter of the cerebellum were used as pseudo-reference regions for the SRTMs. Here, the term “pseudo-reference” region is used as neither the brainstem nor the cerebellum are entirely devoid of $\alpha 5$ subunit specific binding. The methods not relying on a reference region as input were also applied to these regions, but comparison between variants was limited to the six non-reference ROIs only. Regional time-activity curves (TACs) were created by calculation of the mean radioactivity concentration over all grey-matter masked voxels of both left and right hemisphere homologues (excluding the brainstem which is not paired and was not grey-matter masked), for each frame. Likewise, where parametric images

were used, the mean was calculated over all voxels of both homologues (again excluding the brainstem).

2.7. PET data quantification

Where required (one of 10 datasets, based on a maximum translation > 5 mm as estimated using SPM “Realign” function), the dynamic PET images were de-noised and corrected for movement frame-by-frame using wavelets in Piwave 8.0 (Studholme et al., 1997; Turkheimer et al., 1999) running in MATLAB R2014a. The frame starting at 150 s (frame 6) was used as reference due to its high signal-to-noise ratio and the likelihood that the participant had remained still during the first three minutes of the scan. The frames 1–5 were not corrected due to their low signal to noise ratio. The remaining frames (6–24) were automatically resliced and re-concatenated with frames 1–5 into a new dynamic image (Hammers et al., 2007b).

Summation images (also known as ‘add’ or ‘static’ images) were created for frames 1–24, frames 16–21, and frames 22–24 with correction for ¹¹C radiodecay using MICKPM (Modelling, Input functions, and Compartmental Kinetics – Parametric Maps) version 5.4 software (available on request from Rainer Hinz, Wolfson Molecular Imaging Centre, University of Manchester, Manchester, UK), which itself uses MATLAB R2009bSP1. The summation images were required for calculation of global radioactivity concentrations, for use as the reference image during co-registration of the T1-weighted MRI data, and as the input for calculation of SUV images. A binary mask of the brain, which encompassed approximately 9 mm beyond the outer cortical boundary, was also created semi-automatically using Analyze 8.1 (Mayo Clinic, Rochester, New York) for use during the subsequent generation of parametric images.

Quantification of binding was performed as described below, using the same ROIs for each variant. We used a 64-bit PC (Intel Core i5 5300U CPU 2.30 GHz, 8.0 GB RAM) with Windows 7 Enterprise operating system. Variants in which parameters were calculated directly from the ROI TAC data (generated as described in Section 2.6) are henceforth referred to as “regional”. Variants in which parameters were calculated on a voxel-by-voxel basis in order to generate parametric images are referred to as “voxelwise”; in this case the parametric image itself was sampled (mean, standard deviation) within same ROIs as used for regional variants. The quantification methods were:

1. Compartmental models, requiring arterial ppIFs
 - (a) Reversible two-compartment (one tissue compartment) model with two rate constants and variable blood volume (2kbv)
 - (b) Reversible three-compartment (two tissue compartment) model with four rate constants and variable blood volume (4kbv)
2. Graphical analyses, requiring arterial ppIFs
 - (a) Regional Logan's graphical analysis with arterial ppIF
 - (b) Voxelwise Logan's graphical analysis with arterial ppIF
3. Model-free analyses, requiring arterial ppIFs
 - (a) Regional “classic” (non-regularised) SA
 - (b) Voxelwise “classic” SA
4. Methods not requiring arterial ppIFs
 - (a) Voxelwise standardised uptake values (SUVs)
 - (i) 30.5–60.5 min
 - (ii) 60.5–90.5 min
 - (b) Regional SRTM using brainstem
 - (c) Voxelwise SRTM2 using brainstem
 - (d) Regional SRTM using cerebellum
 - (e) Voxelwise SRTM2 using cerebellum

2.8. Weighting of ROI and voxel TACs

For each participant, all ROI/voxel TACs (not yet corrected for decay-correction) were weighted by the same values which were

calculated according to:

$$w_i = \frac{L_i}{T_i} \text{ for frame } (i = 1, 2, 3, \dots, 24; \text{ non - decay corrected data}) \quad (2)$$

[where W_i – weight for frame i ; L_i – length of frame i (seconds); T_i – total of true coincidences (per second) for frame i].

For ROI TACs, the weights were normalised to $\text{sum}(\text{weights})=24$ (i.e. number of frames), thresholded to $\text{max}(\text{weight})\leq 2.5$, and then re-normalised to $\text{sum}(\text{weights})=24$. For voxel TACs, the weights were not normalised but were thresholded to $\text{max}(\text{weight})/\text{min}(\text{weight})\leq 1000$, according to the RPM (Receptor Parametric Mapping software) scheme (Gunn et al., 1998; Aston et al., 2001).

2.9. Reversible compartmental models, requiring arterial ppIFs

MICK (Modelling, Input functions and Compartmental Kinetics) version 5.2 software (available on request from Rainer Hinz, Wolfson Molecular Imaging Centre, University of Manchester, Manchester, UK; see [Supplementary material](#)) was used to fit all regional compartmental models with the Nelder-Mead optimisation algorithm (Nelder and Mead, 1965). MICK uses MATLAB R2009bSP1.

2.9.1. 2kbv

In this model, three microparameters are derived: K_1 , rate constant for influx of the ligand from the plasma to the tissue compartment containing free, non-specifically bound, and specifically bound ligand; k_2 , efflux rate constant from the tissue back to plasma; and bv , the blood volume term. The V_T is then calculated according to the compartmental model equation (Innis et al., 2007).

$$V_T = \frac{K_1}{k_2} \quad (3)$$

We used starting estimates of $K_1=0.01 \text{ ml cm}^{-3} \text{ min}^{-1}$, $k_2=0.001 \text{ min}^{-1}$ and $bv=0.05$.

2.9.2. 4kbv

In addition to K_1 and k_2 (described above for the 2kbv model), two further rate constants were estimated: k_3 , which describes the transfer from the free and non-specifically bound compartment to the specifically bound (second tissue) compartment; and k_4 , which describes the opposite transfer. Again, the blood volume term was also computed. According to the consensus nomenclature (Innis et al., 2007):

$$V_T = \frac{K_1}{k_2} \left(1 + \frac{k_3}{k_4} \right) \quad (4)$$

We used starting estimates of $K_1=0.01 \text{ ml cm}^{-3} \text{ min}^{-1}$, $k_2=0.001 \text{ min}^{-1}$ and $bv=0.05$.

2.10. Graphical analyses, requiring arterial ppIFs

2.10.1. Regional Logan's graphical analysis with arterial ppIF

Logan's graphical analysis (Logan et al., 1990) is a linear analysis applicable to radioligands with reversible binding. After some time (t^*), a plot of

$$\frac{\int_0^t TAC(t') dt'}{TAC(t)} \text{ versus } \frac{\int_0^t ppIF(t') dt'}{TAC(t)} \quad (5)$$

is linear; where $ppIF(t)$ – metabolite-corrected plasma radioactivity concentration at time t , $TAC(t)$ – region of interest radioactivity concentration at time t . For the two-tissue compartment model 4kbv, the slope of the plot is:

$$\frac{K_1}{k_2} \left(1 + \frac{k_3}{k_4} \right) + bv \quad (6)$$

[where bv is the blood volume term], from which V_T can be calculated

as above. MICK was used to fit regional Logan's graphical analyses with the Nelder-Mead optimisation algorithm (Nelder and Mead, 1965). We used fixed parameters of $t^*=1680 \text{ s}$ (i.e. 28 min, based on a preliminary inspection of the plots), $bv=0.028$ (the median across 83 brain regions and the 10 scans, as estimated using 4kbv; interquartile range 0.022–0.036), and equal weights (i.e. each frame was weighted by the same value). The contribution due to vasculature (bv) was subtracted from the ROI TAC prior to the graphical analysis.

2.10.2. Voxelwise Logan's graphical analysis with arterial ppIF

Parametric images of $[^{11}\text{C}]\text{Ro15-4513 } V_T$ were generated from smoothed (isotropic filter with 2.0 mm FWHM) dynamic images and the ppIFs using voxelwise Logan's graphical analysis with ppIF, as implemented in MICKPM, using the same fixed parameters as listed above.

2.11. Model-free analyses, requiring arterial ppIFs

2.11.1. Regional (non-regularised) SA

V_T s for each ROI were obtained from the dynamic images and the ppIFs using SA (Cunningham et al., 1993; Cunningham and Jones, 1993; Turkheimer et al., 1994), as implemented in MICK using the non-negative least squares (NNLS) algorithm (Lawson and Hanson, 1995). The analysis used a base with 100 logarithmically-spaced functions. The fast frequency boundary was kept at the default value of 0.1 s^{-1} . The theoretical slow frequency boundary is based on the decay constant of ^{11}C ($t_{1/2}\approx 20 \text{ min}$, decay constant 0.005663 s^{-1} , $\log_{10}=-3.25$). Based on previous work with tracers with relatively slow kinetics (Hammers et al., 2007b; Riaño Barros et al., 2014) and preliminary investigations (Barros et al., 2010b), we changed this to 0.00063 s^{-1} ($\log_{10}=-3.20$) in order to reduce noise.

2.11.2. Voxelwise SA

Parametric images of $[^{11}\text{C}]\text{Ro15-4513 } V_T$ were generated from the dynamic images and the ppIFs using voxelwise SA as implemented in MICKPM using the NNLS algorithm, with the same number of logarithmic functions and the same fast and slow frequency boundaries as listed above.

2.12. Methods not requiring arterial ppIFs

2.12.1. Voxelwise standardised uptake values (SUVs)

Standardised uptake value images (SUVs) were generated from the decay-corrected summation (add) images in SPM8 for frames 16–21 and for frames 22–24, i.e. from 30.5 to 60.5 and from 60.5 to 90.5 min respectively, according to Kenney et al. (1941):

$$SUV = \frac{\text{radioactivity} \times \text{weight}}{\text{injected dose}} \quad (7)$$

2.12.2. Regional SRTM using brainstem or alternatively using cerebellum

GABA_A receptors are widespread in the brain, and a true reference region devoid of $\alpha 5$ -subunit specific binding does not exist. Attempts have been made to obviate arterial cannulation by using the brain region with the lowest receptor concentration as a pseudo-reference region (Turkheimer et al., 2012). The brainstem and the cerebellum are two of the structures with the lowest concentration of $\alpha 5$ subunits in the human brain (Fritschy and Mohler, 1995; Pirker et al., 2000; Sieghart and Sperk, 2002; Veronese et al., 2016). We therefore used the brainstem and the cerebellum, separately, as a pseudo-reference region in the SRTM (Lammertsma and Hume, 1996) as implemented in MICK, with Nelder-Mead optimisation. We used starting estimates $R_1=0.95$, $k_2a=0.001 \text{ min}^{-1}$ and k_2a' ($k_2\text{RefRegion}$; efflux rate constant from the reference compartment back to plasma) $=0.001 \text{ min}^{-1}$. The

model reduces to the following equation (Wu and Carson, 2002), from which the binding potential (BP_{ND}; (Innis et al., 2007)) can be calculated:

$$C(t) = R_1 C_r(t) + R_1 [k'_{2a} - k_{2a}] C_r(t) * e^{-k_2 t} \quad (8)$$

[where * – convolution operator; C_r(t) – radioactivity concentration in the reference region tissue; C(t) – total radioactivity concentration timecourse in the tissue; k_{2a} – the apparent k₂, i.e. k₂/(1+BP); R₁ – the relative delivery i.e. the ratio K₁/K₁' where K₁' (ml ml⁻¹ min⁻¹) is the rate constant for the influx of the ligand from the plasma to the reference compartment; t – time (min)].

2.12.3. Voxelwise SRTM2 using brainstem or alternatively using cerebellum

Parametric images of BP_{ND} were generated from the dynamic images using a two-step procedure, SRTM2 (Wu and Carson, 2002) with 100 basis functions (Gunn et al., 1997) in MICKPM. Consistent with the SA, we used beta min=0.00063 s⁻¹. We used beta max=0.014 s⁻¹ (similar to Gunn et al., 1997). For each participant, k_{2RefRegion} was set to the global median of k_{2RefRegion} estimates derived from a first-pass SRTM, which itself used the same fixed parameters and a tight brain mask (Wu and Carson, 2002).

2.13. Global radioactivity concentration

Global radioactivity concentrations were calculated for each decay-corrected, summed radioactivity image (frames 01–24) with an in-house script adapted from SPM (Hammers et al., 2007a), where the global radioactivity concentration is defined as the mean voxel value within a mask. The mask itself is defined as all voxels exceeding one-eighth of the mean value of all voxels in the entire image matrix.

2.14. Outcome measures and statistical analyses

2.14.1. Comparison of test and retest injectate data

For the statistical testing we used SPSS for Windows version 22 software (IBM 2013, NY, USA). Injectate data (injected radioactivity, radiochemical purity, co-injected mass of stable ligand, and specific radioactivity at the time of injection) and global radioactivity concentration were compared between test and retest sessions using Student's paired samples *t*-test (for data with a normal distribution) or the non-parametric Wilcoxon signed-rank test (for data which differed significantly from the normal distribution, i.e. Kolmogorov–Smirnov test *p* < 0.05).

2.14.2. Model fit and within-ROI variability

The median residual sum of squares (RSS) was calculated for each ROI, where available (regional variants), as a summary measure of the fit of the model to the observed data. Alternatively, the median within-subject coefficient of variation (WS-CV) was calculated, where available (voxelwise variants), as a summary measure of the within-ROI variability in the binding parameter.

2.14.3. Reproducibility

To assess test – retest variation (i.e. reproducibility), the median (signed and alternatively absolute) percentage difference between test and retest studies as well as their range was calculated for each ROI, for each variant. The (signed) percentage test-retest differences of binding parameters obtained was calculated according to:

$$\text{Test – retest difference} = 200 * \frac{(\text{test value} - \text{retest value})}{(\text{test value} + \text{retest value})} \quad (9)$$

Median absolute percentage test – retest differences (MA-TD) of < 10% were described as “low”; 10% ≤ MA-TD < 15% were described as “moderate”; 15% ≤ MA-TD < 20% were described as “high”; and MA-TD ≥ 20% were described as “very high”.

2.14.4. Reliability

Reliability was calculated using the intraclass correlation coefficient (ICC; (MacLennan, 1993)):

$$ICC = \frac{MSBS - MSWS}{MSBS + (dfWS \times MSWS)} \quad (10)$$

[where MS – mean sum of squares; BS – between-subject; WS – within-subject; and *df* – degrees of freedom]. The ICC is provided to allow assessment of the reliability of the measure as a function of both within-subject variability and between-subject variability; the closer the ICC to 1, the more reliable the variant, i.e. the smaller the within-subject variability of the parameter compared with natural between-subject variability. ICCs were computed in SPSS using the “one-way random” model. We report the “single measures” ICC.

2.14.5. Regional heterogeneity

Finally, the ratio of binding in the highest-binding region (hippocampus) to the lowest-binding non-reference region (occipital lobes) was calculated to allow assessment of each variant's ability to depict the known heterogeneity in α5 subunit availability across the brain. Ratios (“*x*”) of 1.5 ≤ *x* < 1.8 were described as “moderate” heterogeneity; 1.8 ≤ *x* < 2.0 were described as “high” heterogeneity; *x* ≥ 2.0 were described as “very high” heterogeneity.

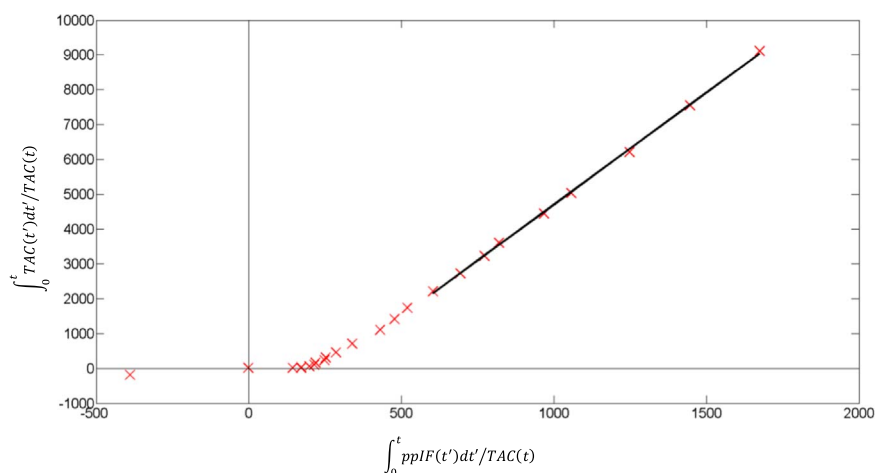


Fig. 1. Example of Logan's graphical analysis plot for a representative participant (2, test scan, for the hippocampus). ppIF(t) – metabolite-corrected plasma radioactivity concentration at time *t*, TAC(t) – region of interest radioactivity concentration at time *t*.

3. Results

3.1. Injectate

Details are given in Table 1. There were no significant differences between test and retest studies in terms of the amount of injected radioactivity (median (range): test 440 (430–452) MBq, retest 441 (435–444) MBq, Student's paired samples *t*-test $p=0.90$); the radiochemical purity (test 99 (96–99)%, retest 98 (98–99)%, Wilcoxon signed-ranks test $p=0.71$); the co-injected mass of stable ligand (test 3.0 (2.0–4.4) μg , retest 2.4 (0.4–5.1) μg , Student's paired samples *t*-test $p=0.78$); or the specific radioactivity at the time of injection (test 49 (26–72) MBq/ ηmol , retest 59 (28–72) MBq/ ηmol , Student's paired samples *t*-test $p=0.66$).

3.2. Global radioactivity concentration

There was no significant difference in global radioactivity concentration between test and retest studies: test 4.65 (range 3.50–5.39) kiloBequerels per millilitre (kBq/ml), retest 4.22 (3.54–4.75) kBq/ml, Student's paired samples *t*-test $p=0.14$.

3.3. Reproducibility and reliability of blood and PET data quantification

See Sections 2 and 3 of the [Supplementary material](#) for details of the parameters derived from the metabolite and plasma-over-blood ratio models, and the six PET quantification methods (12 variants). [Figs. 1 to 5](#) provide examples of the output.

3.4. Comparison between analysis variants

The analyses did not produce any outliers for the ROIs (where "outlier" is defined as V_T or $BP_{ND} \leq 0$ and/or $WS-CV > 50\%$ for regional variants and mean V_T or mean $BP_{ND} \leq 0$ and/or $WS-CV > 100\%$ for voxelwise variants). For well-performing regional variants, there was no evidence of bias or structure in the weighted residuals.

Table 2 provides an overview of the MA-TDs (%) for the six different methods (12 variants). The MA-TDs were very low to low for all SRTM variants and voxelwise SA ($\leq 5\%$); MA-TDs were also low ($< 10\%$) for most ROIs with the 4kbv model. These variants all had very low test-retest differences in the hippocampus ($< 5\%$).

Table 3 provides an overview of the BS-CV (%) for the six different methods (12 variants). The median BS-CVs were moderate for most or all of the ROIs (11–15%) for several variants: 2kbv, 4kbv, voxelwise Logan's graphical analysis, both regional and voxelwise SA, and SUVs (30.5–60.5 and 60.5–90.5 min). The remaining variants, particularly

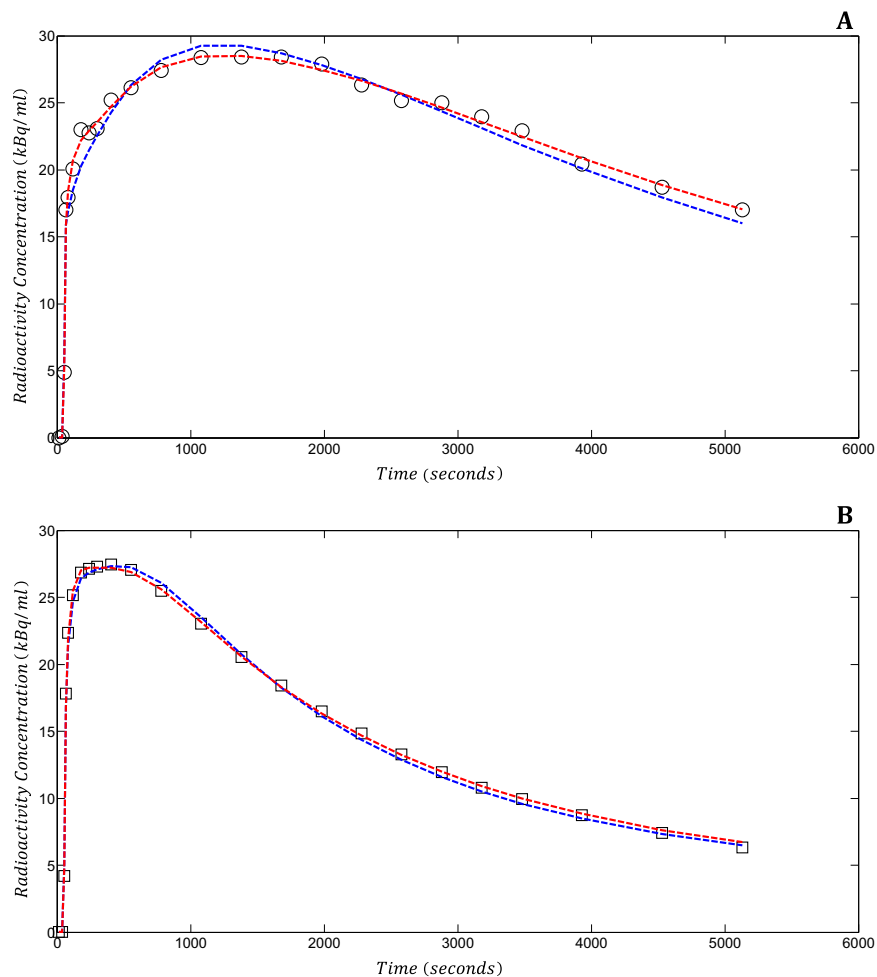


Fig. 2. Example of compartmental model fits for a representative participant (1, retest scan) for the hippocampi (A, circles) and the occipital lobes (B, squares). The 2kbv model is depicted by blue dashed lines, and the 4kbv model is depicted by red dashed lines. The 4kbv model fits better than the 2kbv model in the $\alpha 5$ -subunit-rich hippocampus. 2kbv – reversible one tissue compartment model with variable blood volume; 4kbv – reversible two tissue compartment model with variable blood volume; kBq/ml – kiloBequerels per millilitre. (For interpretation of the references to color in this figure legend, the reader is referred to the web version of this article).

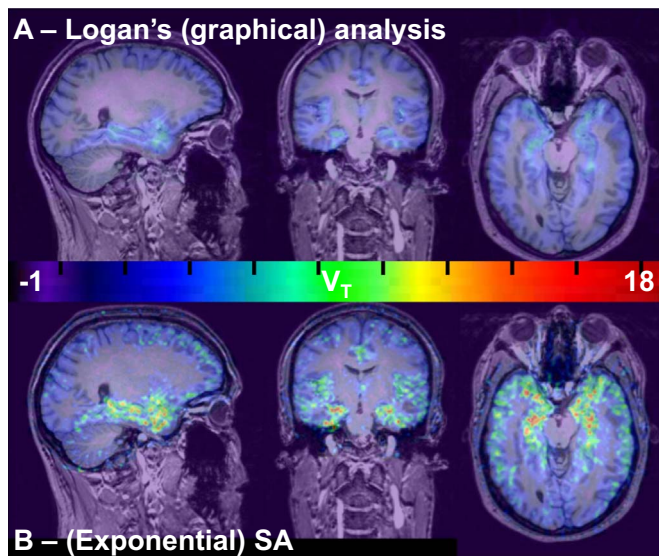


Fig. 3. V_T images for participant 2 (test scan), co-registered to the corresponding T1-weighted MRI image. The images were produced by voxelwise Logan's graphical analysis with ppIF (A – top row), and voxelwise (exponential) SA (B, bottom row). The dynamic data were smoothed (isotropic filter with 2.0 mm FWHM) prior to Logan's graphical analysis. Note the high binding in temporal regions, and the low binding in the cerebellum. Images are shown in radiological orientation (left on right). The colour bar depicts V_T . SA – spectral analysis, V_T – volume-of-distribution. (For interpretation of the references to color in this figure legend, the reader is referred to the web version of this article).

SRTMs using a pseudo-reference region, were characterised by low ($\leq 10\%$) BS-CVs for nearly all ROIs.

Table 4 provides an overview of the ICCs for the six different methods (12 variants). The median ICC was excellent (>0.80) for both the voxelwise SA, and for the voxelwise SRTM2 with the cerebellum as a pseudo-reference region. Regional SRTM using cerebellum also yielded a good (>0.70) median ICC. Other variants yielded low to moderate (≤ 0.70) median ICCs. Regarding the hippocampus, the 4kbv model, voxelwise SA, and both regional and voxelwise SRTM/SRTM2 using cerebellum, and voxelwise SRTM2 using the brainstem all yielded excellent (>0.85) median ICCs. Regional SRTM with the brainstem yielded a very good median (0.77) ICC.

Table 4 also shows the ratio between the hippocampus, which for all variants was the region with highest binding, and a low-binding non-reference region (occipital lobes). Voxelwise SA, regional SRTM using brainstem, and both regional SRTM and voxelwise SRTM2 using the cerebellum all yielded very high ratios (≥ 2.0).

4. Discussion

We describe the test – retest reproducibility and reliability of quantification of the availability of the GABA_A receptor $\alpha 5$ subunit in five healthy human participants. Our major finding is that very good to excellent reproducibility of estimates, in terms of percentage test – retest difference, is achievable using regional and voxelwise implementations of the SRTM and also using model-free, voxelwise SA.

Voxelwise SA was the best-performing variant, in terms of ICCs, and one of the best in terms of percentage test – retest difference. This variant also yielded a slightly higher median BS-CV (11%) than SRTM-based variants, and had a high ratio of hippocampal-to-occipital lobe V_T . We note that voxelwise SA markedly outperformed SA applied to regional TACs. This phenomenon has also been documented for the opioid receptor radioligand [¹¹C]diprenorphine (Hammers et al., 2007b) and the cannabinoid receptor type 1 radioligand, [¹¹C]MePPEP (Riaño Barros et al., 2014). We suggest that the voxelwise

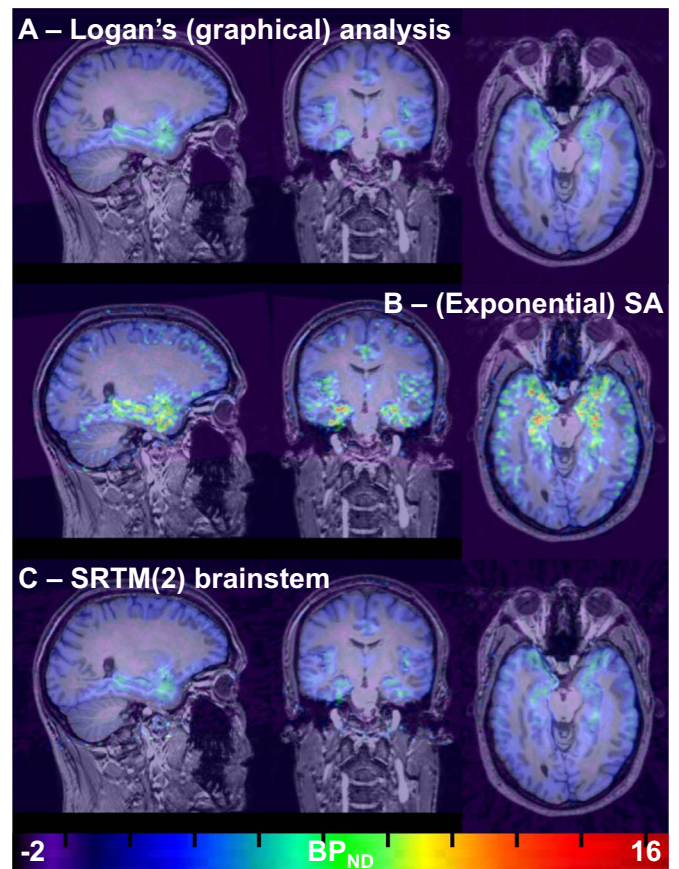


Fig. 4. BP_{ND} images for participant 2 (test scan), co-registered to the corresponding T1-weighted MRI image. For comparison, BP_{ND} images were produced for voxelwise Logan's graphical analysis with ppIF (A – top row) and voxelwise (exponential) SA (B, second row) by dividing the V_T image by the mean of the brainstem (pseudo-reference region) V_T and then subtracting 1. BP_{ND} images are shown for SRTM2 using the brainstem (C – third row) as a pseudo-reference region. The dynamic data were smoothed (isotropic filter with 2.0 mm FWHM) prior to Logan's graphical analysis. Note the high binding in temporal regions, and the low binding in the cerebellum. Images are shown in radiological orientation (left on right). The colour bar depicts BP_{ND} . BP_{ND} – binding potential relative to non-displaceable binding, ppIF – (arterial) parent plasma input function; SA – spectral analysis, V_T – volume-of-distribution. (For interpretation of the references to color in this figure legend, the reader is referred to the web version of this article).

approach benefits from the flexibility to be able to accommodate differences in blood volume, tissue class partial volume and receptor concentration between voxels, in contrast to variants that use the averaged regional TAC.

The assumptions inherent to SA are that: 1) the compartmental systems are strongly connected; 2) the exchange of material with the environment is confined to a single compartment; and 3) there is no possibility for material to pass from one compartment through two or more compartments back to the initial compartment (Schmidt, 1999). There is no evidence to indicate that SA is biased towards or against any particular patient population. An arterial input function is required, as the fit assumes a sum of positive series of convolution integrals of the input function. One advantage of SA is that it is “data driven”, i.e. *a priori* model selection is not required. Like all voxel-based methods, the generation of parametric V_T images via voxelwise SA has the added advantage of allowing whole-brain surveys in diseases where the exact localisation of pathology is not known, e.g. refractory focal epilepsy.

Of the compartmental models, the 2kbv model had a very high median percentage test – retest variability (MA-TD; 25%); whilst the 4kbv model had an acceptable MA-TD (8%). However, a wide range of percentage test – retest variability was observed across participants for

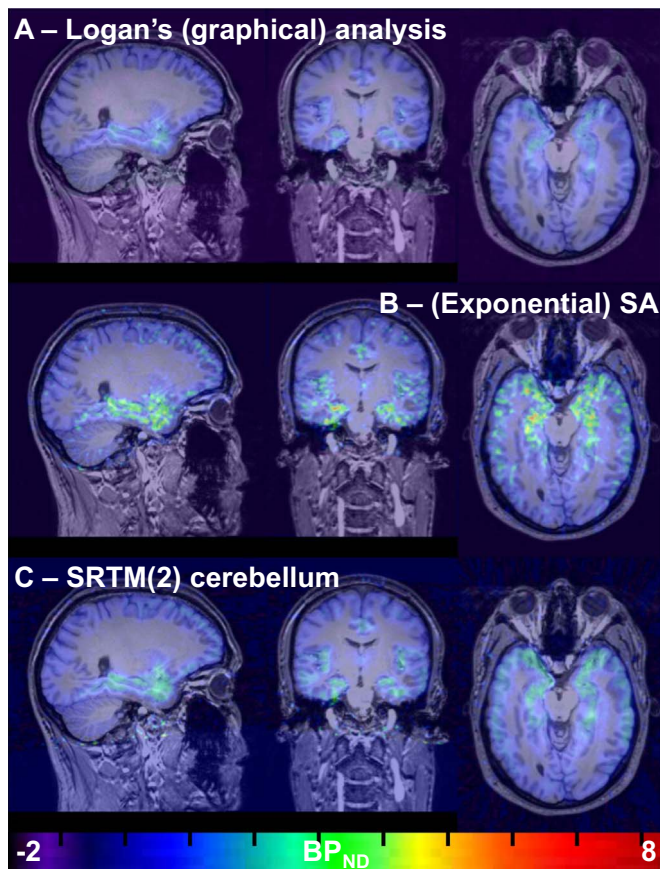


Fig. 5. BP_{ND} images for participant 2 (test scan), co-registered to the corresponding T1-weighted MRI image. For comparison, BP_{ND} images were produced for voxelwise Logan's graphical analysis with ppIF (A – top row) and voxelwise (exponential) SA (B, second row) by dividing the V_T image by the mean of the cerebellum (pseudo-reference region) V_T and then subtracting 1. BP_{ND} images are shown for SRTM2 using the cerebellum (C, bottom row) as a pseudo-reference region. The dynamic data were smoothed (isotropic filter with 2.0 mm FWHM) prior to Logan's graphical analysis. Note the high binding in temporal regions, and the low binding in the cerebellum. Images are shown in radiological orientation (left on right). The colour bar depicts BP_{ND} . BP_{ND} – binding potential relative to non-displaceable binding, ppIF – (arterial) parent plasma input function; SA – spectral analysis, V_T – volume-of-distribution. (For interpretation of the references to color in this figure legend, the reader is referred to the web version of this article.).

each region, other than in the hippocampus (3%, range –2–7%). These data are in keeping with previous findings, in which the fits with two-tissue compartment models were better than those seen with one-tissue compartment models (Asai et al., 2009; Myers et al., 2012; Myers et al., 2012, 2016).

While [^{11}C]Ro15-4513 has highest affinity for GABA_A receptors containing $\alpha 5$ subunits (Lingford-Hughes et al., 2002), it also binds to GABA_A receptors containing $\alpha 1$ and other α subunits, albeit with approximately 10–15 times lower affinity (Hadingham et al., 1993; Luddens et al., 1994; Myers et al., 2012; Stokes et al., 2013). Recently, human heterologous competition data acquired from healthy males using the $\alpha 5$ -subunit-selective negative allosteric modulator, Basmisanil (RG1662), suggested that $\alpha 5$ -specific binding accounts for 60–70% of the specific binding in most regions (Myers et al., 2016). As the regional distribution of α subunits overlaps, the tissue kinetics, model fits and hence reliability will vary according to the proportion of subunits (Maeda et al., 2003; Myers et al., 2012). Model-free quantification, such as with SA, offers flexibility to deal with the complex compartmentalisation of the radioligand targets (Myers et al., 2012; Riaño Barros et al., 2014).

Logan's graphical analyses had a very high MA-TD, whether applied to regional TACs or on a voxel-by-voxel basis. It is possible that more than nine frames are required to accurately fit the plot, although we did smooth the dynamic images before voxelwise analyses. Also, the analyses assumed a fixed blood volume contribution of 0.028, the median derived from multiple regions and scans, which cannot be correct for each ROI in each participant.

In the present study, we quantified the total V_T , rather than attempting to isolate the presumed $\alpha 5$ -subunit-specific volume-of-distribution (V_s), for example via bandpass SA (Stokes et al., 2014). However, accurate isolation of the V_s is challenging and is vulnerable to the effects of tissue heterogeneity and noise. Whilst V_s appears to exhibit a tight relationship with the 'true' $\alpha 5$ -subunit-specific V_T in regions with moderate or high $\alpha 5$ subunit concentration, the total V_T also exhibits a tight, linear association (Myers et al., 2016).

As expected, our analyses revealed that the reproducibility of [^{11}C]Ro15-4513 V_T was sensitive to multiple methodological choices, e.g. derivation of the input function and method used to calculate the weighting factors (e.g. Yaqub et al., 2006; data not shown).

Non-invasive PET studies are preferable in both research and clinical studies, in order to avoid the discomfort and slight risks attributable to arterial cannulation, a procedure which demands expertise. GABA_A receptor $\alpha 5$ subunits are expressed throughout the brain, and a true reference region does not exist. Here we used the brainstem and alternatively the cerebellum as pseudo-reference regions, based on their near-negligible expression of the $\alpha 5$ subunit (Fritschy and Mohler, 1995; Pirker et al., 2000; Sieghart and Sperk, 2002; Veronese et al., 2016). This approach is supported by recent data that suggest the V_s is low in the cerebellum and extremely low in the pons (Myers et al., 2016). In the present study, both variants yielded reproducible data, in terms of percentage test – retest difference, whether applied to regional TACs or on a voxel-by-voxel basis. BS-CV was low, however, which perhaps reflects a bias of the reference region methods. The actual BP_{ND} values were much lower for the SRTMs when using cerebellum as the pseudo-reference rather than the brainstem, which probably reflects greater $\alpha 5$ -subunit-specific binding in the former (Myers et al., 2016). A wider range of percentage test – retest difference was seen for the brainstem than for the cerebellum with compartmental models. We observed lower signal-to-noise ratio, i.e. noisier time-activity curves, for the smaller brainstem ROI, which impaired model fitting.

Whilst the recent Basmisanil (RG1662) blocking study found a tight, linear relationship between BP_{ND} and the 'true' $\alpha 5$ -subunit-specific volume-of-distribution with both variants (Myers et al., 2016), SRTMs should only be used if even very small intra- or between-subject variations in the amount of GABA_A receptor-specific binding in these pseudo-reference regions can be excluded. It might be possible to improve on these results by utilising a sub-region of the brainstem or cerebellum, or via a more sophisticated pseudo-reference region approach (e.g. Turkheimer et al., 2012).

SUVs can constitute a simple and reliable measure of radioligand binding that obviates the need for arterial blood sampling (Riaño Barros et al., 2014). In the present study, [^{11}C]Ro15-4513 SUVs were moderately reproducible overall (median MA-TD 11%), but had a wide range in percentage test – retest difference for most regions. The SUVs were moderately reliable (median ICC 0.70), which is partly attributable to the large BS-CV (median 15%). Overall these data suggest that factors other than weight and injected dose significantly influence reproducibility. Given the performance of voxelwise SA with arterial input function, and the moderately-high MA-TD we observed in the area under the metabolite model curve (12%, see Supplementary material, Table 2), we hypothesise that such factors include the rate of metabolism of the parent radioligand.

The present study is limited by the sample size; in particular ICCs must be treated with caution when using paired data acquired from eight or less participants (Walter et al., 1998; Shoukri et al., 2004). As

Table 2
MA-TDs (median absolute t-rt differences (%)) for participants' parameter estimates ($BP_{ND}/SUV/V_T$) obtained with the six different methods (12 variants).

Method	2kbv	4kbv	Logan's graphical analysis	Logan's graphical analysis	SA	SA	SUV (30.5–60.5 min)	SUV (60.5–90.5 min)	SRTM brainstem	SRTM2 brainstem	SRTM cerebellum	SRTM2 cerebellum
Parameter	V_T	V_T	V_T	V_T	V_T	V_T	SUV	SUV	BP_{ND}	BP_{ND}	BP_{ND}	BP_{ND}
Regional/Voxelwise	Regional	Regional	Regional	Voxelwise	Regional	Voxelwise	Voxelwise	Voxelwise	Regional	Voxelwise	Regional	Voxelwise
ACG	28	7	18	19	10	4	11	21	5	6	2	1
Fusiform gyrus	28	14	19	20	14	10	10	15	8	6	5	4
Hippocampus	22	3	13	9	6	2	6	16	3	2	3	2
Inferior frontal gyrus	17	5	8	9	7	5	11	14	5	5	5	4
Insula	27	8	16	17	14	1	12	20	7	6	3	2
Occipital lobes	21	8	17	15	15	8	13	17	4	1	5	3
Median (iqr)	25 (21–28)	8 (6–8)	17 (14–18)	16 (11–19)	12 (8–14)	5 (3–7)	11 (10–12)	17 (15–19)	5 (4–7)	6 (3–6)	4 (3–5)	3 (2–4)

2/4kbv=2/4 rate constant compartmental models with variable blood volume, ACG=Anterior cingulate gyrus, BP_{ND} =Binding potential relative to non-displaceable binding, iqr=Interquartile range, SUV=Standardised uptake value, ROI=Region-of-interest, SA=Spectral analysis, SRTM=Simplified reference tissue model, t-rt=test-retest, V_T =Volume-of-distribution.

Table 3
Mean between-subject coefficients of variation (BS-CV; %) for participants' parameter estimates ($BP_{ND}/SUV/V_T$) obtained with the six different methods (12 variants).

Method	2kbv	4kbv	Logan's graphical analysis	Logan's graphical analysis	SA	SA	SUV (30.5–60.5 min)	SUV (60.5–90.5 min)	SRTM brainstem	SRTM2 brainstem	SRTM cerebellum	SRTM2 cerebellum
Parameter	V_T	V_T	V_T	V_T	V_T	V_T	SUV	SUV	BP_{ND}	BP_{ND}	BP_{ND}	BP_{ND}
Regional/Voxelwise	Regional	Regional	Regional	Voxelwise	Regional	Voxelwise	Voxelwise	Voxelwise	Regional	Voxelwise	Regional	Voxelwise
ACG	15	9	12	12	10	10	16	20	5	5	8	8
Fusiform gyrus	15	26	12	12	14	14	14	19	5	6	7	8
Hippocampus	15	9	10	11	12	11	13	18	8	9	8	11
Inferior frontal gyrus	12	20	10	10	15	12	18	22	8	8	9	10
Insula	14	11	10	10	10	10	14	18	6	6	7	8
Occipital lobes	11	18	9	10	14	10	19	21	7	7	9	9
Median (iqr)	15 (13–15)	15 (10–20)	10 (10–12)	11 (10–12)	13 (11–14)	11 (10–12)	15 (14–18)	20 (18–21)	7 (5–8)	7 (6–8)	8 (7–9)	9 (8–10)

2/4kbv=2/4 rate constant compartmental models with variable blood volume, ACG=Anterior cingulate gyrus, BP_{ND} =Binding potential relative to non-displaceable binding, iqr=Interquartile range, SUV=Standardised uptake value, ROI=Region-of-interest, SA=Spectral analysis, SRTM=Simplified reference tissue model, t-rt=test-retest, V_T =Volume-of-distribution.

the free fraction of parent radioligand in the plasma was not quantified, we cannot comment on the reproducibility or reliability of BP_f or V_T (Innis et al., 2007). However, voxelwise SA based on arterial ppIFs that were not corrected for plasma free fraction still yielded reproducible and reliable V_T data. The test – retest scan interval was short, but varied from a week to two months between participants; this variable was not associated with reproducibility.

The lack of females in our study population is an additional limitation. To the best of our knowledge, the potential influence of the menstrual cycle on the availability of the GABA_A receptor or of the $\alpha 5$ subunit in particular has not been studied. However, the menstrual cycle influences GABA concentration in the frontal lobe, as measured by proton magnetic resonance spectroscopy (e.g. Harada et al., 2011; De Bondt et al., 2015), which could conceivably lower test – retest reproducibility. Hence, confirmation of our findings in women would

be desirable.

5. Conclusions

Quantification of [¹¹C]Ro15-4513 binding shows very good to excellent reproducibility with SRTMs and voxelwise SA. Quantification of binding in the $\alpha 5$ -subunit-rich hippocampus is particularly reliable. Whilst SA necessitates arterial blood sampling, it is preferable to the SRTMs due to the lack of a true reference region. [¹¹C]Ro15-4513 PET is well-placed as a tool to study the availability of the GABA_A receptor $\alpha 5$ subunit in health and neuropsychiatric disease.

Conflicts of interest

The authors do not report any conflicts of interest.

Table 4
Intraclass Correlation Coefficients (ICCs) for participants' parameter estimates (BP_{ND}/SUV/V_T) obtained with the six different methods (12 variants).

Method	2kbv		4kbv		Logan's graphical analysis		Logan's graphical analysis		SA		SA		SUV (30.5–60.5 min)		SUV (60.5–90.5 min)		SRTM brainstem		SRTM2 brainstem		SRTM cerebellum		SRTM2 cerebellum	
	V _T	Regional	V _T	Regional	V _T	Regional	V _T	Regional	V _T	Voxelwise	V _T	Voxelwise	SUV	Voxelwise	SUV	Voxelwise	BP _{ND}	Regional	BP _{ND}	Voxelwise	BP _{ND}	Regional	BP _{ND}	Voxelwise
ACG	-0.24	0.64	0.08	0.08	0.00	0.32	0.91	0.59	0.62	-0.33	-0.18	0.66	0.62	0.62	0.65	0.62	0.59	-0.33	-0.18	0.59	-0.18	0.59	-0.33	0.66
Fusiform gyrus	-0.38	0.45	-0.08	-0.08	-0.12	0.60	0.71	0.67	0.65	0.22	0.27	0.64	0.65	0.65	0.65	0.65	0.68	0.22	0.27	0.68	0.27	0.68	0.22	0.64
Hippocampus	-0.52	0.89	-0.07	-0.07	-0.10	0.35	0.89	0.72	0.72	0.77	0.85	0.93	0.72	0.72	0.72	0.72	0.95	0.77	0.85	0.95	0.85	0.95	0.77	0.93
Inferior frontal gyrus	-0.41	-0.01	-0.01	-0.01	-0.02	0.40	0.88	0.76	0.75	0.63	0.66	0.87	0.75	0.75	0.75	0.75	0.87	0.63	0.66	0.87	0.66	0.87	0.63	0.87
Insula	-0.55	0.51	-0.21	-0.21	-0.22	-0.73	0.90	0.60	0.63	0.22	0.34	0.84	0.60	0.60	0.63	0.63	0.74	0.22	0.34	0.74	0.34	0.74	0.22	0.84
Occipital lobes	-0.65	0.36	-0.30	-0.30	-0.30	-0.18	0.59	0.72	0.68	0.46	0.50	0.81	0.72	0.68	0.68	0.68	0.63	0.46	0.50	0.63	0.50	0.63	0.46	0.81
Median (Iqr)	-0.47 (-0.54 to -0.39)	0.48 (-0.38 to 0.61)	-0.08 (-0.03 to 0.03)	-0.08 (-0.18 to 0.03)	-0.11 (-0.20 to -0.04)	0.34 (-0.06 to 0.39)	0.89 (0.75–0.90)	0.70 (0.62–0.72)	0.67 (0.64–0.71)	0.67 (0.64–0.71)	0.34 (0.22–0.59)	0.42 (0.29–0.62)	0.71 (0.64–0.84)	0.67 (0.64–0.71)	0.67 (0.64–0.71)	0.67 (0.64–0.71)	0.71 (0.64–0.84)	0.34 (0.22–0.59)	0.42 (0.29–0.62)	0.71 (0.64–0.84)	0.42 (0.29–0.62)	0.71 (0.64–0.84)	0.42 (0.29–0.62)	0.83 (0.70–0.86)
Hippocampus /Occipital lobes	1.7	1.9	1.8	1.8	1.8	1.8	2.2	1.9	2.5	2.1	1.9	2.5	2.5	2.5	2.5	3.2	2.1	1.9	3.2	1.9	3.2	2.1	2.8	

2/4kbv=2/4 rate constant compartmental models with variable blood volume, ACG=Anterior cingulate gyrus, BP_{ND}=Binding potential relative to non-displaceable binding, Iqr=Interquartile range, SUV=Standardised uptake value, ROI=Region-of-interest, SA=Spectral analysis, SRTM=Simplified reference tissue model, t-rt=test-retest, V_T=Volume-of-distribution.

Acknowledgments

We thank the staff of Hammersmith Imanet Limited and the Hammersmith Hospital MRI Unit for their assistance with data acquisition and preparation. This study was supported by the Medical Research Council (MRC) Clinical Sciences Centre (MC_U120085812). Authors affiliated with (1) are grateful for support from the Department of Health National Institute of Health Research Biomedical Research Centre funding scheme. CJM was supported by an MRC Doctoral Training Account (3+1) studentship that was awarded by Imperial College London. MJK was supported by the Epilepsy Society, University College London (UCL), UCL Hospitals (UCLH) and UCLH/UCL Biomedical Research Centre. AH was supported by an MRC Clinician Scientist Fellowship (G108/585) and the Neurodis Foundation. We are very grateful to the anonymous Reviewers, whose comments helped us to improve the quality of this manuscript.

Appendix A. Supplementary material

Supplementary data associated with this article can be found in the online version at <http://dx.doi.org/10.1016/j.neuroimage.2016.12.038>.

References

Allen, E.V., 1929. Thromboangiitis obliterans: methods of diagnosis of chronic occlusive arterial lesions distal to the wrist with illustrative cases. *Am. J. Med. Sci.* 178, 237–244.

Asai, Y., Takano, A., Ito, H., Okubo, Y., Matsuura, M., Otsuka, A., Takahashi, H., Ando, T., Ito, S., Arakawa, R., Asai, K., Suhara, T., 2008. GABAA/Benzodiazepine receptor binding in patients with schizophrenia using [¹¹C]Ro15-4513, a radioligand with relatively high affinity for alpha5 subunit. *Schizophr. Res.* 99, 333–340.

Asai, Y., Ikoma, Y., Takano, A., Maeda, J., Toyama, H., Yasuno, F., Ichimiya, T., Ito, H., Suhara, T., 2009. Quantitative analyses of [¹¹C]Ro15-4513 binding to subunits of GABAA/benzodiazepine receptor in the living human brain. *Nucl. Med. Commun.* 30, 872–880.

Aston, J., Worsley, K., Gunn, R., 2001. RPM statistics – a statistical tool for receptor parametric mapping. *NeuroImage* 13, 65.

Barnard, E.A., Skolnick, P., Olsen, R.W., Mohler, H., Sieghart, W., Biggio, G., Braestrup, C., Bateson, A.N., Langer, S.Z., 1998. International Union of Pharmacology. XV. Subtypes of gamma-aminobutyric acid A receptors: classification on the basis of subunit structure and receptor function. *Pharmacol. Rev.* 50, 291–313.

Barros, D.A.R., Heckemann, R.A., Keihaninejad, S., McGinnity, C.J., Gousias, I.S., Duncan, J.S., Koeppe, M.J., Brooks, D.J., Hammers, A., 2010a. Toward investigating the causes of memory difficulties in temporal lobe epilepsy: a study using the novel alpha5 GABA(A) receptor PET ligand C-11 RO15 4513. *Epilepsia* 51, 136–136.

Barros, D.A.R., Heckemann, R.A., Rosso, L., McGinnity, C.J., Keihaninejad, S., Gousias, I.S., Brooks, D.J., Duncan, J.S., Koeppe, M.J., Turkheimer, F.E., Hammers, A., 2010b. Investigating the reproducibility of the novel alpha-5 GABAA receptor PET ligand 11C Ro15 4513. *NeuroImage* 52, S112.

Bonetti, E.P., Burkard, W.P., Gabl, M., Hunkeler, W., Lorez, H.P., Martin, J.R., Moehler, H., Osterrieder, W., Pieri, L., Polc, P., Richards, J.G., Schaffner, R., Scherschlicht, R., Schoch, P., Haefely, W.E., 1988. Ro 15-4513: partial inverse agonism at the BZR and interaction with ethanol. *Pharmacol. Biochem. Behav.* 31, 733–749.

Brunig, I., Scotti, E., Sidler, C., Fritschy, J.M., 2002. Intact sorting, targeting, and clustering of gamma-aminobutyric acid A receptor subtypes in hippocampal neurons in vitro. *J. Comp. Neurol.* 443, 43–55.

Cable, D.G., Mullany, C.J., Schaff, H.V., 1999. The Allen test. *Ann. Thorac. Surg.* 67, 876–877.

Carascos, V.B., Elliott, E.M., You-Ten, K.E., Cheng, V.Y., Bellelli, D., Newell, J.G., Jackson, M.F., Lambert, J.J., Rosahl, T.W., Wafford, K.A., MacDonald, J.F., Orser, B.A., 2004. Tonic inhibition in mouse hippocampal CA1 pyramidal neurons is mediated by alpha5 subunit-containing gamma-aminobutyric acid type A receptors. *Proc. Natl. Acad. Sci. U S A* 101, 3662–3667.

Charych, E.I., Liu, F., Moss, S.J., Brandon, N.J., 2009. GABA(A) receptors and their associated proteins: implications in the etiology and treatment of schizophrenia and related disorders. *Neuropharmacology* 57, 481–495.

Cheng, V.Y., Martin, L.J., Elliott, E.M., Kim, J.H., Mount, H.T., Taverna, F.A., Roder, J.C., Macdonald, J.F., Bhabri, A., Collinson, N., Wafford, K.A., Orser, B.A., 2006. Alpha5 GABAA receptors mediate the amnesic but not sedative-hypnotic effects of the general anesthetic etomidate. *J. Neurosci.* 26, 3713–3720.

Collinson, N., Kuenzi, F.M., Jarolimek, W., Maubach, K.A., Cuthill, R., Sur, C., Smith, A., Otu, F.M., Howell, O., Atack, J.R., McKernan, R.M., Seabrook, G.R., Dawson, G.R., Whiting, P.J., Rosahl, T.W., 2002. Enhanced learning and memory and altered GABAergic synaptic transmission in mice lacking the alpha 5 subunit of the GABAA receptor. *J. Neurosci.* 22, 5572–5580.

Crestani, F., Keist, R., Fritschy, J.-M., Benke, D., Vogt, K., Prut, L., Blüthmann, H., Möhler, H., Rudolph, U., 2002. Trace fear conditioning involves hippocampal alpha

- GABAA receptors. *Proc. Natl. Acad. Sci. U S A* 99, 8980–8985.
- Cunningham, V., Ashburner, J., Byrne, H., Jones, T., 1993. Use of spectral-analysis to obtain parametric images from dynamic pet studies. In: *Proceedings of International Symposium on Quantification of Brain Function*, Akita, Japan.
- Cunningham, V.J., Jones, T., 1993. Spectral analysis of dynamic PET studies. *J. Cereb. Blood Flow Metab.* 13, 15–23.
- Curtis, D.R., Felix, D., McLellan, H., 1970. GABA and hippocampal inhibition. *Br. J. Pharmacol.* 40, 881–883.
- Dawson, G.R., Maubach, K.A., Collinson, N., Cobain, M., Everitt, B.J., MacLeod, A.M., Choudhury, H.I., McDonald, L.M., Pillai, G., Rycroft, W., Smith, A.J., Sternfeld, F., Tattersall, F.D., Wafford, K.A., Reynolds, D.S., Seabrook, G.R., Atack, J.R., 2006. An inverse agonist selective for $\alpha 5$ subunit-containing GABAA receptors enhances cognition. *J. Pharmacol. Exp. Ther.* 316, 1335–1345.
- De Bondt, T., De Belder, F., Vanhevel, F., Jacquemyn, Y., Parizel, P.M., 2015. Prefrontal GABA concentration changes in women-Influence of menstrual cycle phase, hormonal contraceptive use, and correlation with premenstrual symptoms. *Brain Res.* 1597, 129–138.
- Defrise, M., Kinahan, P.E., Townsend, D.W., Michel, C., Sibomana, M., Newport, D.F., 1997. Exact and approximate rebinning algorithms for 3-D PET data. *IEEE Trans. Med. Imaging* 16, 145–158.
- Fritschy, J.M., Mohler, H., 1995. GABAA-receptor heterogeneity in the adult rat brain: differential regional and cellular distribution of seven major subunits. *J. Comp. Neurol.* 359, 154–194.
- Galanopoulou, A.S., 2008. GABA(A) receptors in normal development and seizures: friends or foes? *Curr. Neuropharmacol* 6, 1–20.
- Gonzalez, M.I., Brooks-Kayal, A., 2011. Altered GABA(A) receptor expression during epileptogenesis. *Neurosci. Lett.* 497, 218–222.
- Gousias, I.S., Rueckert, D., Heckemann, R.A., Dyet, L.E., Boardman, J.P., Edwards, A.D., Hammers, A., 2008. Automatic segmentation of brain MRIs of 2-year-olds into 83 regions of interest. *NeuroImage* 40, 672–684.
- Gunn, R.N., Lammertsma, A.A., Hume, S.P., Cunningham, V.J., 1997. Parametric imaging of ligand-receptor binding in PET using a simplified reference region model. *NeuroImage* 6, 279–287.
- Gunn, R.N., Sargent, P.A., Bench, C.J., Rabiner, E.A., Osman, S., Pike, V.W., Hume, S.P., Grasby, P.M., Lammertsma, A.A., 1998. Tracer kinetic modeling of the 5-HT1A receptor ligand [carbonyl-11C]WAY-100635 for PET. *NeuroImage* 8, 426–440.
- Hadingham, K.L., Wingrove, P.B., Wafford, K.A., Bain, C., Kemp, J.A., Palmer, K.J., Wilson, A.W., Wilcox, A.S., Sikela, J.M., Ragan, C.I., et al., 1993. Role of the beta subunit in determining the pharmacology of human gamma-aminobutyric acid type A receptors. *Mol. Pharmacol.* 44, 1211–1218.
- Hammers, A., Allom, R., Koeppe, M.J., Free, S.L., Myers, R., Lemieux, L., Mitchell, T.N., Brooks, D.J., Duncan, J.S., 2003. Three-dimensional maximum probability atlas of the human brain, with particular reference to the temporal lobe. *Hum. Brain Mapp.* 19, 224–247.
- Hammers, A., Asselin, M.C., Hinz, R., Kitchen, I., Brooks, D.J., Duncan, J.S., Koeppe, M.J., 2007a. Upregulation of opioid receptor binding following spontaneous epileptic seizures. *Brain* 130, 1009–1016.
- Hammers, A., Asselin, M.C., Turkheimer, F.E., Hinz, R., Osman, S., Hotton, G., Brooks, D.J., Duncan, J.S., Koeppe, M.J., 2007b. Balancing bias, reliability, noise properties and the need for parametric maps in quantitative ligand PET: [¹¹C]diprenorphine test-retest data. *NeuroImage* 38, 82–94.
- Hammers, A., Panagoda, P., Heckemann, R.A., Kelsch, W., Turkheimer, F.E., Brooks, D.J., Duncan, J.S., Koeppe, M.J., 2008. [¹¹C] Flumazenil PET in temporal lobe epilepsy: do we need an arterial input function or kinetic modeling? *J. Cereb. Blood Flow Metab.* 28, 207–216.
- Harada, M., Kubo, H., Nose, A., Nishitani, H., Matsuda, T., 2011. Measurement of variation in the human cerebral GABA level by in vivo MEGA-editing proton MR spectroscopy using a clinical 3 T instrument and its dependence on brain region and the female menstrual cycle. *Hum. Brain Mapp.* 32, 828–833.
- Heckemann, R.A., Hajnal, J.V., Aljabar, P., Rueckert, D., Hammers, A., 2006. Automatic anatomical brain MRI segmentation combining label propagation and decision fusion. *NeuroImage* 33, 115–126.
- Heckemann, R.A., Keihaninejad, S., Aljabar, P., Rueckert, D., Hajnal, J.V., Hammers, A., 2010. Improving intersubject image registration using tissue-class information benefits robustness and accuracy of multi-atlas based anatomical segmentation. *NeuroImage* 51, 221–227.
- Hinz, R., Bhagwagar, Z., Cowen, P.J., Cunningham, V.J., Grasby, P.M., 2007. Validation of a tracer kinetic model for the quantification of 5-HT2A receptors in human brain with [¹¹C]MDL 100,907. *J. Cereb. Blood Flow Metab.* 27, 161–172.
- Innis, R.B., Cunningham, V.J., Delforge, J., Fujita, M., Gjedde, A., Gunn, R.N., Holden, J., Houle, S., Huang, S.C., Ichise, M., Iida, H., Ito, H., Kimura, Y., Koeppe, R.A., Knudsen, G.M., Knuuti, J., Lammertsma, A.A., Laruelle, M., Logan, J., Maguire, R.P., Mintun, M.A., Morris, M.D., Parsey, R., Price, J.C., Slifstun, M., Sossi, V., Suhara, T., Votaw, J.R., Wong, D.F., Carson, R.E., 2007. Consensus nomenclature for in vivo imaging of reversibly binding radioligands. *J. Cereb. Blood Flow Metab.* 27, 1533–1539.
- Inoue, O., Suhara, T., Itoh, T., Kobayashi, K., Suzuki, K., Tateno, Y., 1992. In vivo binding of [¹¹C]Ro15-4513 in human brain measured with PET. *Neurosci. Lett.* 145, 133–136.
- Kenney, J.M., Marinelli, L., Woodard, H.Q., 1941. Tracer studies with radioactive phosphorus in malignant neoplastic disease. *Radiology* 37, 683–690.
- Korpi, E.R., Sinkkonen, S.T., 2006. GABA(A) receptor subtypes as targets for neuropsychiatric drug development. *Pharmacol. Ther.* 109, 12–32.
- Lammertsma, A.A., Hume, S.P., 1996. Simplified reference tissue model for PET receptor studies. *NeuroImage* 4, 153–158.
- Lawson, C.L., Hanson, R.J., 1995. *Solving Least Squares Problems*. Society for Industrial and Applied Mathematics (SIAM), Philadelphia, USA. <http://dx.doi.org/10.1137/1.9781611971217>.
- Lingford-Hughes, A., Hume, S.P., Feeney, A., Hirani, E., Osman, S., Cunningham, V.J., Pike, V.W., Brooks, D.J., Nutt, D.J., 2002. Imaging the GABA-benzodiazepine receptor subtype containing the alpha5-subunit in vivo with [¹¹C]Ro15 4513 positron emission tomography. *J. Cereb. Blood Flow Metab.* 22, 878–889.
- Lingford-Hughes, A., Reid, A.G., Myers, J., Feeney, A., Hammers, A., Taylor, L.G., Rosso, L., Turkheimer, F., Brooks, D.J., Grasby, P., Nutt, D.J., 2012. A [¹¹C]Ro15 4513 PET study suggests that alcohol dependence in man is associated with reduced alpha5 benzodiazepine receptors in limbic regions. *J. Psychopharmacol.* 26, 273–281.
- Lister, R.G., Nutt, D.J., 1988. Interactions of the imidazodiazepine Ro 15-4513 with chemical convulsants. *Br. J. Pharmacol.* 93, 210–214.
- Lobo, I.A., Harris, R.A., 2008. GABA(A) receptors and alcohol. *Pharmacol. Biochem. Behav.* 90, 90–94.
- Logan, J., Fowler, J.S., Volkow, N.D., Wolf, A.P., Dewey, S.L., Schlyer, D.J., MacGregor, R.R., Hitzemann, R., Bendriem, B., Gatley, S.J., et al., 1990. Graphical analysis of reversible radioligand binding from time-activity measurements applied to [¹¹C-methyl]-(-)-cocaine PET studies in human subjects. *J. Cereb. Blood Flow Metab.* 10, 740–747.
- Lou, H.C., Rosenstand, A., Brooks, D.J., Bender, D., Jakobsen, S., Blicher, J.U., Hansen, K.V., Moller, A., 2016. Exogenous dopamine reduces GABA receptor availability in the human brain. *Brain Behav.*, e00484.
- Luddens, H., Seeburg, P.H., Korpi, E.R., 1994. Impact of beta and gamma variants on ligand-binding properties of gamma-aminobutyric acid type A receptors. *Mol. Pharmacol.* 45, 810–814.
- Macdonald, R.L., Gallagher, M.J., Feng, H.J., Kang, J., 2004. GABA(A) receptor epilepsy mutations. *Biochem. Pharmacol.* 68, 1497–1506.
- MacLennan, R.N., 1993. Interrater reliability with SPSS for windows 5.0. *The Am. Stat.* 47, 292–296.
- Maeda, J., Suhara, T., Kawabe, K., Okauchi, T., Obayashi, S., Hojo, J., Suzuki, K., 2003. Visualization of alpha5 subunit of GABAA/benzodiazepine receptor by 11C Ro15-4513 using positron emission tomography. *Synapse* 47, 200–208.
- Mendez, M.A., Horder, J., Myers, J., Coghill, S., Stokes, P., Erritzoe, D., Howes, O., Lingford-Hughes, A., Murphy, D., Nutt, D., 2013. The brain GABA-benzodiazepine receptor alpha-5 subtype in autism spectrum disorder: a pilot [¹¹C]Ro15-4513 positron emission tomography study. *Neuropharmacology* 68, 195–201.
- Myers, J.F., Rosso, L., Watson, B.J., Wilson, S.J., Kalk, N.J., Clementi, N., Brooks, D.J., Nutt, D.J., Turkheimer, F.E., Lingford-Hughes, A.R., 2012. Characterisation of the contribution of the GABA-benzodiazepine alpha1 receptor subtype to [¹¹C]Ro15-4513 PET images. *J. Cereb. Blood Flow Metab.* 32, 731–744.
- Myers, J.F., Comley, R.A., Gunn, R.N., 2016. Quantification of [¹¹C]Ro15-4513 GABA A alpha5 specific binding and regional selectivity in humans. *J. Cereb. Blood Flow Metab.* pii: 0271678X16661339. [Epub ahead of print].
- Nelder, J.A., Mead, R., 1965. A simplex method for function minimization. *The Computer Journal* 7, 308–313.
- Nutt, D.J., Besson, M., Wilson, S.J., Dawson, G.R., Lingford-Hughes, A.R., 2007. Blockade of alcohol's amnesic activity in humans by an $\alpha 5$ subtype benzodiazepine receptor inverse agonist. *Neuropharmacology* 53, 810–820.
- Pirker, S., Schwarzer, C., Wieselthaler, A., Sieghart, W., Sperk, G., 2000. GABA(A) receptors: immunocytochemical distribution of 13 subunits in the adult rat brain. *Neuroscience* 101, 815–850.
- Ranica, A.S., Williams, C.W., Schnorr, L., Clark, J.C., Rhodes, C.G., Bloomfield, P.M., Jones, T., 1991. The on-line monitoring of continuously withdrawn arterial blood during PET studies using a single BGO/photomultiplier assembly and non-stick tubing. *Med. Prog. Technol.* 17, 259–264.
- Riaño Barros, D.A., McGinnity, C.J., Rosso, L., Heckemann, R.A., Howes, O.D., Brooks, D.J., Duncan, J.S., Turkheimer, F.E., Koeppe, M.J., Hammers, A., 2014. Test-retest reproducibility of cannabinoid-receptor type 1 availability quantified with the PET ligand [¹¹C]MePEP. *NeuroImage* 97, 151–162.
- Roy-Byrne, P.P., 2005. The GABA-benzodiazepine receptor complex: structure, function, and role in anxiety. *J. Clin. Psychiatry* 66 (Suppl 2), S14–S20.
- Sadzot, B., Frost, J.J., Wagner, H.N., Jr., 1989. In vivo labeling of central benzodiazepine receptors with the partial inverse agonist [³H]Ro 15-4513. *Brain Res.* 491, 128–135.
- Schmidt, K., 1999. Which linear compartmental systems can be analyzed by spectral analysis of PET output data summed over all compartments? *J. Cereb. Blood Flow Metab.* 19, 560–569.
- Shoukri, M.M., Asyali, M.H., Donner, A., 2004. Sample size requirements for the design of reliability study: review and new results. *Stat. Methods Med. Res.* 13, 251–271.
- Sieghart, W., Sperk, G., 2002. Subunit composition, distribution and function of GABA(A) receptor subtypes. *Curr. Top. Med. Chem.* 2, 795–816.
- Slogoff, S., Keats, A.S., Arlund, C., 1983. On the safety of radial artery cannulation. *Anesthesiology* 59, 42–47.
- Spinks, T.J., Jones, T., Bloomfield, P.M., Bailey, D.L., Miller, M., Hogg, D., Jones, W.F., Vaigneur, K., Reed, J., Young, J., Newport, D., Moyers, C., Casey, M.E., Nutt, R., 2000. Physical characteristics of the ECAT EXACT3D positron tomograph. *Phys. Med. Biol.* 45, 2601–2618.
- Sternfeld, F., Carling, R.W., Jelley, R.A., Ladduwahetty, T., Merchant, K.J., Moore, K.W., Reeve, A.J., Street, L.J., O'Connor, D., Sohal, B., Atack, J.R., Cook, S., Seabrook, G., Wafford, K., Tattersall, F.D., Collinson, N., Dawson, G.R., Castro, J.L., MacLeod, A.M., 2004. Selective, orally active gamma-aminobutyric acid A alpha5 receptor inverse agonists as cognition enhancers. *J. Med. Chem.* 47, 2176–2179.
- Stokes, P.R., Benecke, A., Myers, J., Erritzoe, D., Watson, B.J., Kalk, N., Barros, D.R., Hammers, A., Nutt, D.J., Lingford-Hughes, A.R., 2013. History of cigarette smoking is associated with higher limbic GABAA receptor availability. *NeuroImage* 69, 70–77.
- Stokes, P.R., Myers, J.F., Kalk, N.J., Watson, B.J., Erritzoe, D., Wilson, S.J.,

- Cunningham, V.J., Riano Barros, D., Hammers, A., Turkheimer, F.E., Nutt, D.J., Lingford-Hughes, A.R., 2014. Acute increases in synaptic GABA detectable in the living human brain: a [^{11}C]Ro15-4513 PET study. *NeuroImage* 99, 158–165.
- Studholme, C., Hill, D.L., Hawkes, D.J., 1997. Automated three-dimensional registration of magnetic resonance and positron emission tomography brain images by multiresolution optimization of voxel similarity measures. *Med. Phys.* 24, 25–35.
- Sur, C., Quirk, K., Dewar, D., Atack, J., McKernan, R., 1998. Rat and human hippocampal alpha5 subunit-containing gamma-aminobutyric AcidA receptors have alpha5 beta3 gamma2 pharmacological characteristics. *Mol. Pharmacol.* 54, 928–933.
- Turkheimer, F., Moresco, R.M., Lucignani, G., Sokoloff, L., Fazio, F., Schmidt, K., 1994. The use of spectral analysis to determine regional cerebral glucose utilization with positron emission tomography and [^{18}F]fluorodeoxyglucose: Theory, implementation, and optimization procedures. *J. Cereb. Blood Flow Metab.* 14, 406–422.
- Turkheimer, F.E., Brett, M., Visvikis, D., Cunningham, V.J., 1999. Multiresolution analysis of emission tomography images in the wavelet domain. *J. Cereb. Blood Flow Metab.* 19, 1189–1208.
- Turkheimer, F.E., Selvaraj, S., Hinz, R., Murthy, V., Bhagwagar, Z., Grasby, P., Howes, O., Rosso, L., Bose, S.K., 2012. Quantification of ligand PET studies using a reference region with a displaceable fraction: application to occupancy studies with [^{11}C]-DASB as an example. *J. Cereb. Blood Flow Metab.* 32, 70–80.
- Veronese, M., Zanotti-Fregonara, P., Rizzo, G., Bertoldo, A., Innis, R.B., Turkheimer, F.E., 2016. Measuring specific receptor binding of a PET radioligand in human brain without pharmacological blockade: The genomic plot. *NeuroImage* 130, 1–12.
- Walter, S.D., Eliasziw, M., Donner, A., 1998. Sample size and optimal designs for reliability studies. *Stat. Med.* 17, 101–110.
- Wu, Y., Carson, R.E., 2002. Noise reduction in the simplified reference tissue model for neuroreceptor functional imaging. *J. Cereb. Blood Flow Metab.* 22, 1440–1452.
- Yaqub, M., Boellaard, R., Kropholler, M.A., Lammertsma, A.A., 2006. Optimization algorithms and weighting factors for analysis of dynamic PET studies. *Phys. Med. Biol.* 51, 4217–4232.
- Yee, B.K., Hauser, J., Dolgov, V.V., Keist, R., Mohler, H., Rudolph, U., Feldon, J., 2004. GABA receptors containing the alpha5 subunit mediate the trace effect in aversive and appetitive conditioning and extinction of conditioned fear. *Eur. J. Neurosci.* 20, 1928–1936.